Inelastic neutron scattering, lattice dynamics and high-pressure phase stability in $LuPO_4$ and $YbPO_4$

2007 J. Phys.: Condens. Matter 19 446202

(http://iopscience.iop.org/0953-8984/19/44/446202)

IOP PUBLISHING JOURNAL OF PHYSICS: CONDENSED MATTER

J. Phys.: Condens. Matter **19** (2007) 446202 (13pp) doi:10.1088/0953-8984/19/44/446202

Inelastic neutron scattering, lattice dynamics and high-pressure phase stability in $LuPO_4$ and $YbPO_4$

R Mittal[1,3], **S L Chaplot**[1], **N Choudhury**[1] **and C-K Loong**[1,2]

[1] Solid State Physics Division, Bhabha Atomic Research Centre, Trombay, Mumbai 400 085, India
[2] Intense Pulsed Neutron Source Division, Argonne National Laboratory, IL 60439, USA

Received 3 August 2007, in final form 18 September 2007
Published 16 October 2007
Online at stacks.iop.org/JPhysCM/19/446202

Abstract

The combination of physical and chemical properties of orthophosphates, such as high melting point, structural and chemical stability and long-term corrosion resistance, makes them an ideal medium for the storage and permanent disposal of nuclear waste materials. We have carried out lattice dynamical studies using a shell model based on transferable interatomic potential for $LuPO_4$ and $YbPO_4$ in their zircon and scheelite phases. We also report inelastic neutron scattering measurements of the phonon density of states for $YbPO_4$. The calculations in the zircon phase are in good agreement with the reported experimental data on phonon density of states and phonon dispersion relation for $LuPO_4$ and our data for $YbPO_4$. The lattice dynamical model is found to be useful for the calculation of various thermodynamic properties such as the specific heat, thermal expansion and equation of state in both zircon and scheelite phases of these compounds. The calculated free energy in zircon and scheelite phases shows their relative stability below and above 22 GPa, respectively.

(Some figures in this article are in colour only in the electronic version)

1. Introduction

The high melting temperature, structural and chemical stability and long-term corrosion resistance of rare-earth orthophosphates have prompted the suggestion of their use as a nuclear waste storage medium [1]. Moreover, orthophosphates have been the subject of several magnetic and optical studies because of their use as x-ray and gamma-ray scintillators for medical imaging application [2]. The compounds of the second half of the lanthanide series starting with the Tb member crystallize in the zircon structure [3, 4] at ambient conditions. High-pressure Raman spectroscopic and x-ray diffraction studies have been reported [5–8] for rare-earth orthovanadates ($DyVO_4$, $TbVO_4$ and YVO_4) and $LuPO_4$. The measurements show a zircon to scheelite type structural phase transition. Strong electron–phonon coupling has been observed [9] in electronic Raman spectra of $YbPO_4$. Elastic constant measurement by the

[3] Present address: Forschungszentrum Jülich GmbH, Jülich Centre for Neutron Science, c/o TU München, Lichtenbergstr 1, 85747 Garching, Germany.

Brillouin scattering technique was reported in $LuPO_4$ first at room temperature [10a] and then in both $LuPO_4$ and $YbPO_4$ from 10 to 300 K [10b]. The temperature dependence of $(C_{11}–C_{12})$ for $YbPO_4$ shows nearly 20% softening, believed to be due to the presence of electron–phonon coupling between the rare-earth magnetic moment and the lattice. In contrast, in $LuPO_4$ there is no interaction between electrons and phonons because of the completely filled 4f shell in Lu^{3+}. The dynamic response of 4f electron–lattice interactions in $YbPO_4$ has been characterized by inelastic neutron scattering measurements [11] on a single-crystal sample.

Phonon properties are important for understanding the thermodynamic behavior of these materials under natural radiation damage and temperature–pressure conditions prevalent in the earth's crust. For zircon structure MPO_4 compounds, only the long-wavelength Raman and infrared modes have been reported [12, 13], with the exception of neutron scattering measurements of the phonon density of states and phonon dispersion relations of $LuPO_4$ using polycrystalline and single-crystal specimens [14]. Lattice dynamical calculations have also been reported [14] for $LuPO_4$ using a shell model involving adjustable force constant parameters. Force constant models developed at ambient pressure are not useful for the calculations of thermodynamic properties at high pressures. Recently, we have reported extensive phonon studies [15–18] in mineral zircon, $ZrSiO_4$. In this paper we report the measurement of phonon density of states for $YbPO_4$ using the HRMECS spectrometer at Argonne National Laboratory. These measurements on $YbPO_4$ and extensive phonon data for $LuPO_4$ available in the literature [14] are used for developing transferable interatomic potential models for these compounds. We have calculated various phonon properties and free energies in the zircon and scheelite phases and thereby the phase diagram of $LuPO_4$. The details of the structure and group theoretical analysis of phonon modes are given in section 2. Section 3 describes the experimental technique. The lattice dynamic calculations are outlined in section 4, while the results and discussion and the conclusions are presented in sections 5 and 6, respectively.

2. Structure and group theoretical analysis

Lanthanide orthophosphates can be divided into two groups on the basis of their crystal structure. Orthophosphates formed by the first half of the series (La to Gd) have monazite structure and the remaining half has the zircon structure at ambient pressure. $YbPO_4$ and $LuPO_4$ belong to the latter group of orthophosphates and their structure [3, 4] consists (figure 1) of four formula units in a body-centered tetragonal unit cell (space group $I4_1/amd$).

The group theoretical analysis of the phonon dispersion relation in the zircon phase of $YbPO_4$ and $LuPO_4$ has been carried out using standard techniques [19]. The symmetry decompositions of the phonon branches at the Γ point and along the Δ, Λ and Σ directions are given as

$$\Gamma: \quad 2A_{1g} + A_{2g} + A_{1u} + 4A_{2u} + 4B_{1g} + B_{2g} + B_{1u} + 2B_{2u} + 5E_g + 5E_u$$
$$\Delta: \quad 8\Delta_1 + 8\Delta_2 + 10\Delta_3 + 10\Delta_4$$
$$\Lambda: \quad 6\Lambda_1 + 2\Lambda_2 + 6\Lambda_3 + 2\Lambda_4 + 10\Lambda_5$$
$$\Sigma: \quad 10\Sigma_1 + 8\Sigma_2 + 10\Sigma_3 + 8\Sigma_4.$$

The A_{1g}, B_{1g} and E_g modes are Raman active while the A_{2u} and E_u modes are infrared (IR) active. The A_{2g}, A_{1u}, B_{1u} and B_{2u} modes are optically inactive. The results of group theoretical analysis have been used to block diagonalize the dynamical matrices in lattice dynamical calculations and to label the various phonon branches. There are 36 distinct dispersion branches along the [100] and [110] directions, while along [001] the number of distinct branches is only 26 due to the degeneracy of phonons of Δ_5 representation.

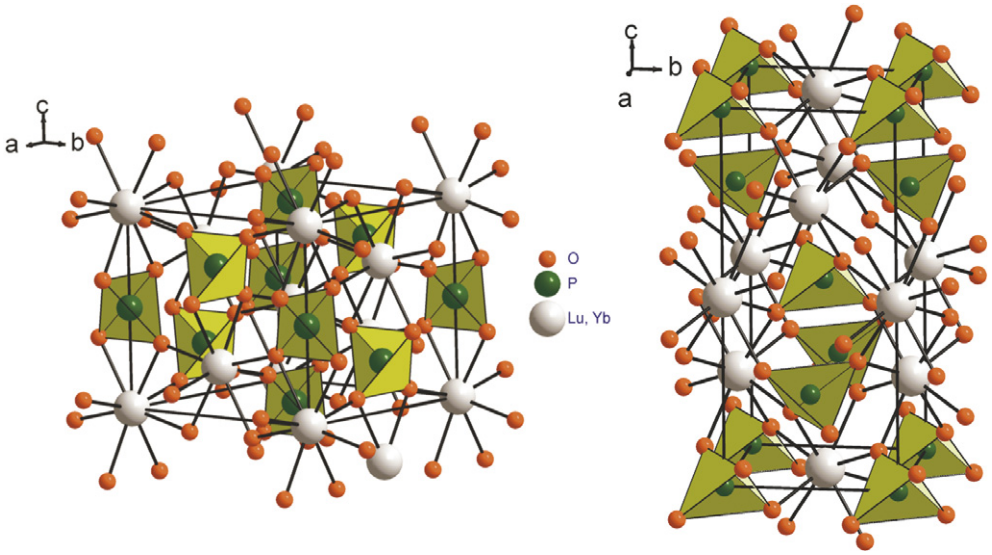

Figure 1. The representation of the zircon (space group $I4_1/amd$) and scheelite ($I4_1/a$) phases of MPO_4 (M = Lu, Yb).

3. Experimental details

The inelastic neutron scattering experiments were performed using the High-Resolution Medium-Energy Chopper Spectrometer (HRMECS) at the Intense Pulse Neutron Source (IPNS) of Argonne National Laboratory. The time of flight HRMECS spectrometer is equipped with wide-angular-coverage multi-detector banks. The energy resolution of the HRMECS spectrometer varies from about 4% of E_0 in the elastic region to about 2% near the end of the neutron energy-loss spectrum. A polycrystalline sample of about 40 g was placed in an planar aluminum container. The container was mounted at a 45° angle to the incident beam. Such geometry limits the neutron traverse length in the sample for all detector angles to 1–2 mm, thereby reducing multiple-scattering effects. To reduce multiphonon scattering the measurements were carried out at 15 K. Background scattering was subtracted from the data using empty container runs. Measurements of elastic incoherent scattering from a vanadium sample provided detector calibration and intensity normalization. The incident energy of the neutron (E_0) was 200 meV. This allows measurements of the inelastic scattering signal over a wide range of momentum transfer (Q). Under these conditions the neutron-cross-section-weighted phonon density of states $g^{(n)}(E)$ can be reliably obtained from the experiments under the incoherent approximation [20]. One has

$$g^{(n)}(E) = A\left\langle \frac{\mathrm{e}^{2W(Q)}}{Q^2} \frac{E}{n(E,T)+1} S(Q,E) \right\rangle.$$

Since measurements are carried out at low temperature, variations in $W(Q)$ may be neglected. Then

$$g^{(n)}(E) \simeq B \sum_p \frac{4\pi b_p^2}{M_p} g_p(E) \tag{1}$$

where $n(E,T) = [\exp(E/KT) - 1]^{-1}$.

Table 1. Potential parameters used in the lattice dynamical calculations.

	Lu	Yb	P	O
$Z(k)$	2.971	2.971	3.013	−1.496
$R(k)$ (Å)	1.954	1.968	0.749	1.835

Here, A and B are normalization constants, and b_p, M_p and $g_p(E)$ are respectively the neutron scattering length, mass and partial density of states of the pth atom in the unit cell. The factor $4\pi b_p^2/M_p$ for Lu, Yb, P and O atoms is 0.041, 0.135, 0.107 and 0.265 barns/amu, respectively. The quantity within $\langle\text{—}\rangle$ represents the average over all Q values. $2W(Q)$ is the Debye–Waller factor.

4. Lattice dynamical calculations

We have used a pair potential consisting of Coulombic and Born–Mayer type short-ranged repulsive interaction terms and a van der Waals type attractive interaction between the oxygen atoms. The potential energy is given by

$$V(r_{kk'}) = \frac{e^2}{4\pi\epsilon_0}\frac{Z(k)Z(k')}{r_{kk'}} + a\exp\left(\frac{-br_{kk'}}{R(k)+R(k')}\right) - \frac{C}{r_{kk'}^6}, \tag{2}$$

where $Z(k)$ and $R(k)$ are the effective charge and radius of the kth type of atom. $Z(k)$, $R(k)$ and C are empirical parameters and $a = 1822$ eV and $b = 12.364$ are constants. We have successfully used this set of parameters in the lattice dynamical calculations for several complex solids [21–24]. The radii and charge parameters used for the calculations are given in table 1. The van der Waals interaction (last term) in equation (2) is applied only between the O–O pairs. The value of C chosen is 21.61 eV Å^6. In addition to the interactions given by equation (2) we have also introduced a P–O stretch potential of the form

$$V(r) = -D\exp[-n(r-r_0)^2/(2r)] \tag{3}$$

with parameters $D = 1.66$ eV, $n = 29.8$ Å^{-1}, $r_0 = 1.534$ Å. The polarizability of the oxygen atoms is introduced in the framework of the shell model [25, 26] with the shell charge $Y(\text{O}) = -2.54$ and shell–core force constant $K(\text{O}) = 110$ eV Å^{-2}. The criteria for optimizing the empirical parameters are (a) to produce the minimum-enthalpy structure close to that determined by diffraction experiments at ambient pressure; (b) to yield consistently only real calculated phonon frequencies from lattice dynamical calculations and (c) to conform with the experimentally determined long wavelength phonon modes and elastic constants. At high pressure, we first determined the minimum enthalpy structure at each pressure using the above potential and then used the same in quasiharmonic lattice dynamical calculations. The calculations have been carried out using the latest version of software DISPR [27] developed at Trombay. We note the limitation in transferring the model to $YbPO_4$ in view of the electron–phonon interaction. However, we would like to examine the suitability of the model for $YbPO_4$.

5. Results and discussion

5.1. Raman and infrared modes, inelastic neutron scattering, total and partial phonon density of states and phonon dispersion relation

The comparison between the calculated and experimental [12, 13] long-wavelength Raman and infrared modes for $LuPO_4$ and $YbPO_4$ (table 2) shows that the average deviation of our

Table 2. Comparison of the calculated and experimental long-wavelength Raman [12] and infrared [13] modes in cm^{-1} units (1 cm^{-1} = 0.124 meV) for $LuPO_4$ and $YbPO_4$. The A_{2g}, A_{1u}, B_{1u} and B_{2u} modes are optically inactive.

	$LuPO_4$			$YbPO_4$	
	Expt	Calc. [14]	Calc.	Expt	Calc.
A_{1g}	493	481	483	491	483
	1011	1017	1034	1009	1033
A_{2g}			245		243
B_{1g}	138	135	140	132	141
			338		336
	670	683	671	663	671
	1069	1082	1068	1068	1068
B_{2g}	334	318	320	330	321
E_g	144	130	141	138	142
	191	189	188		187
	308	309	282	302	281
	587	586	582	582	582
	1032	1036	1005	1030	1004
A_{1u}			465		464
A_{2u}(LO)	372	363	393		393
	673	652	653		653
	1192	1128	1152		1151
A_{2u}(TO)	266	276	244		245
	634	625	622		622
	1062	1080	1071		1071
B_{1u}			157		156
B_{2u}			564		563
			1020		1020
E_u(LO)	273	267	292		292
	358	362	347		345
	537	545	536		537
	1125	1066	1058		1057
E_u(TO)	207	198	182		182
	347	353	346		344
	517	510	484		485
	1000	1013	969		969

calculations from the experimental data is 4.5%. The maximum discrepancy (8.5%) is in one of the Raman active modes around 308 cm^{-1} (=38.2 meV) and 302 cm^{-1} (=37.5 meV) in $LuPO_4$ and $YbPO_4$ respectively. The large LO–TO splitting (table 2) for the A_{2u} and E_u modes has been correctly described by our calculation. Overall, there is a good agreement between the calculated and the measured values of optical frequencies. The calculated zone center phonon modes for $LuPO_4$ using the force constant model of Nipko *et al* [14] are also given in table 2.

The comparison between the calculated and experimental data [14] of phonon dispersion relation available in the literature for $LuPO_4$ along (100), (001) and (110) is shown in figure 2. The calculations are in reasonably good agreement with the experimental data. However, there are some discrepancies between the calculations and experimental data for the optic modes around 40 meV along the directions [100] and [110].

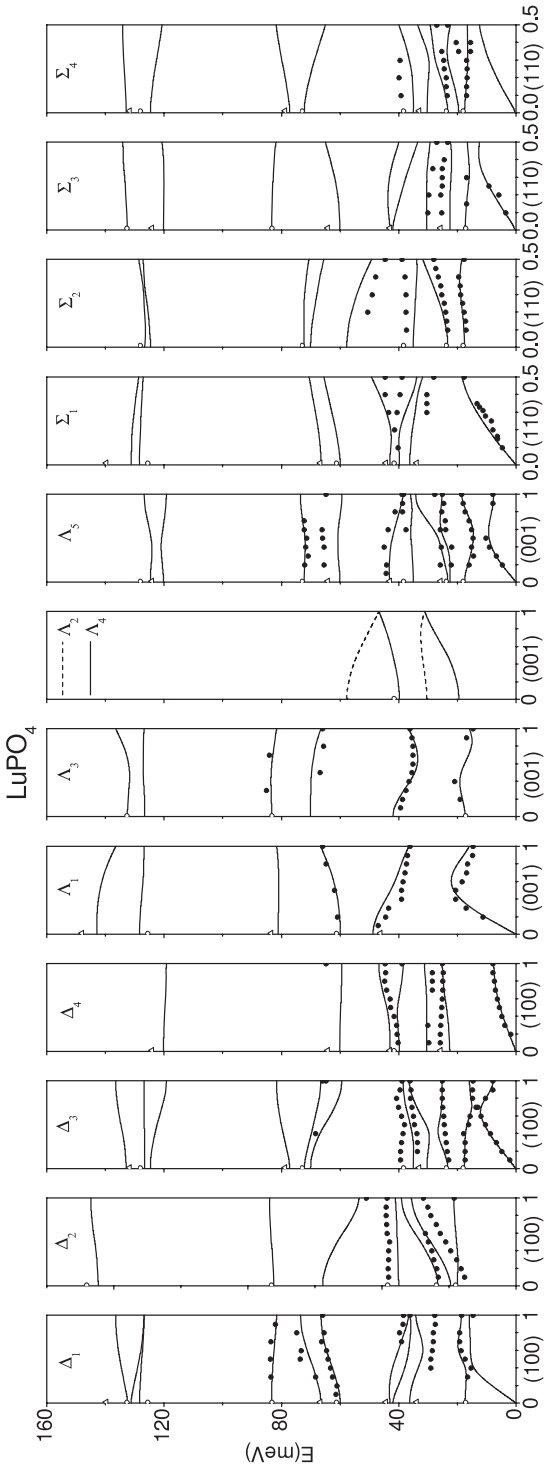

Figure 2. Comparison between the calculated (lines) and experimental (symbols) phonon dispersion relations of $LuPO_4$ in the zircon phase. The open circles, open triangles and closed circles indicate Raman [12], infrared [13] and neutron [14] data respectively.

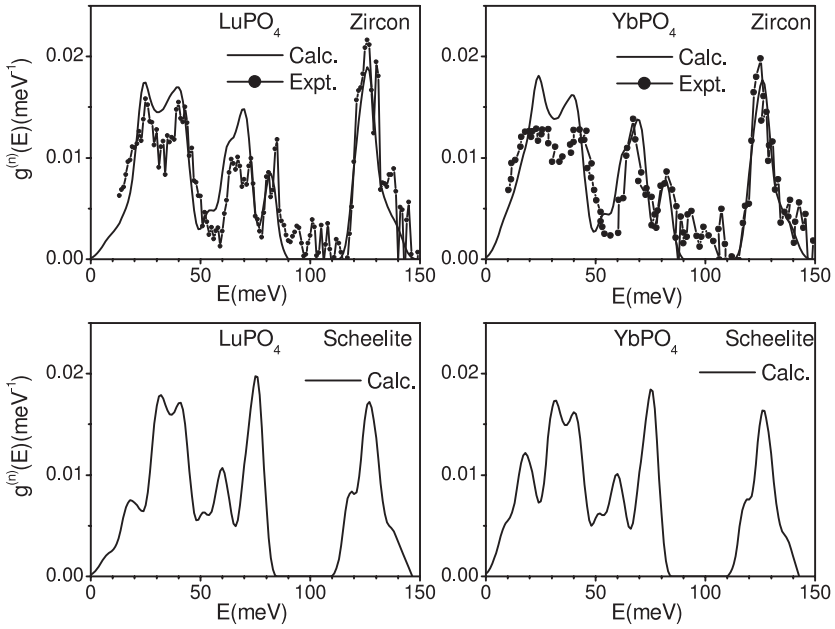

Figure 3. Comparison between the experimental and calculated phonon density of states of $YbPO_4$ and $LuPO_4$ [14] in the zircon phase. A Gaussian of FWHM 6 meV has been used for the smoothing in order to correspond to the energy resolution in the experiment (which varies between 2 and 4% of the incident energy of 200 meV). The calculated phonon density of states for the scheelite phase is also shown in the lower panel. The experimental neutron-weighted one-phonon density of states is obtained by subtracting the calculated multiphonon contribution from the experimental data. The multiphonon contribution is obtained using the Sjolander formalism [28].

The contribution from 729 wavevectors has been included in calculation of the phonon density of states (figure 3). The histogram sampling of frequencies is carried out in a frequency interval of 1.0 meV. The calculated neutron-weighted one-phonon density of states (figure 3) is in good agreement with our measured data on $YbPO_4$ and the reported data [14] for $LuPO_4$. The spectra consist of phonon bands centered at about 24, 40, 68, 83 and 125 meV. There is a band gap in the energy range of 90–115 meV. These can be interpreted in terms of the partial density of states contributed from various atomic species. The calculated partial density of states (figure 4) shows that rare-earth atoms contribute below 50 meV. The phonon band around 24 meV is broader in $YbPO_4$ as compared to that in $LuPO_4$ due to a dominant broad contribution from the Yb atom. The vibrations of oxygen and phosphate atoms span the entire 0–145 meV range. Above 115 meV the contributions are mainly due to P–O stretching modes. The total phonon densities of states for $LuPO_4$ and $YbPO_4$ are very similar due to the fact that the compounds are isostructural and the masses of the rare-earth elements (Yb and Lu) are nearly same. The presence of strong electron–phonon interaction in $YbPO_4$ may also result in some broadening in the experimental data of neutron-weighted phonon density of states in the 0–40 meV energy range. However, due to a different scattering length of Yb (0.137 fm) in comparison with Lu (0.076 fm), it is difficult to unambiguously attribute the observed broadening in the phonon bands to electron–phonon interaction.

We have also calculated partial densities of states of various atoms in the scheelite phase (figure 4) of $YbPO_4$ and $LuPO_4$. The total density of states in both zircon and scheelite phases is similar. However, the band gap (85–120 meV) of the zircon phase is shifted towards lower energy in the scheelite phase.

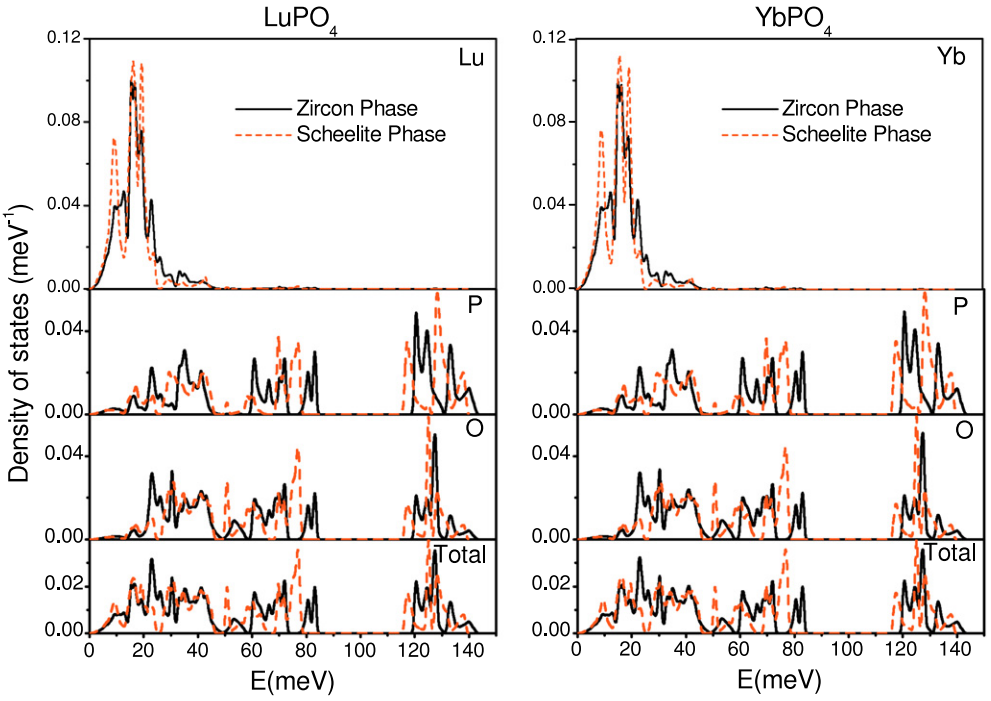

Figure 4. Calculated partial densities of states of various atoms in $LuPO_4$ and $YbPO_4$.

5.2. Elastic constants, thermodynamic properties and high-pressure phase transitions

The calculated elastic constants (obtained from the slopes of the acoustic phonon branches near the zone center) (table 3) at ambient pressure are found to be in fairly good agreement with the experimental data [10]. We have also calculated the elastic constants (table 3) in the scheelite phase. The calculated values of elastic constants for $LuPO_4$ and $YbPO_4$ are nearly identical. There is a strong departure between calculations and experiments in $YbPO_4$, especially for C_{33}, C_{66} and C_{12}. As the present model does not take into account the interactions with electrons, especially between the Yb^{3+} f electrons and acoustic phonons in $YbPO_4$, it is likely that the electron–phonon coupling might influence these elastic constants.

The experimental data of the equation of state are not available for $LuPO_4$ and $YbPO_4$. The lattice dynamical model is used for the predictions of bulk modulus and equation of state (figure 5). The calculated bulk modulus values at ambient pressure for the zircon (scheelite) phase of $LuPO_4$ and $YbPO_4$ are 184 GPa (195 GPa) and 181 GPa (199 GPa) respectively.

The calculated phonon density of states $g(E)$ is used to compute the lattice specific heat as a function of temperature. The specific heat at constant volume is given by

$$C_V = \frac{\mathrm{d}}{\mathrm{d}T} \int \mathrm{d}E\, g(E)(n + 1/2)E, \tag{4}$$

where $n = [\exp(\frac{E}{K_B T}) - 1]^{-1}$.

The C_P–C_V correction to the specific heat, arising from anharmonicity of phonons, is given by

$$C_P - C_V = \alpha_V^2 BVT, \tag{5}$$

where α_V, B and V are the volume thermal expansion coefficient, bulk modulus and volume of the crystal, respectively.

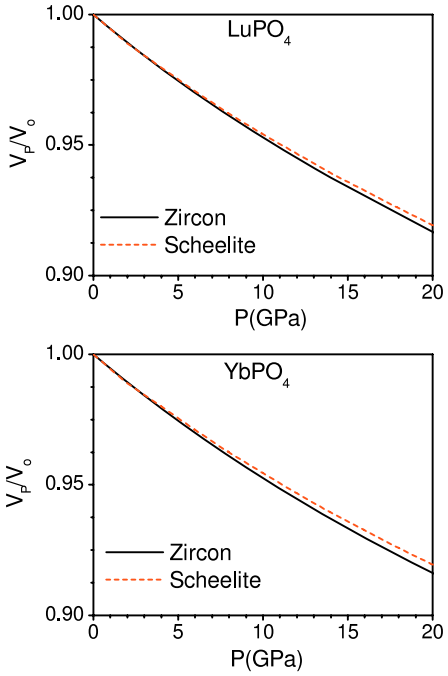

Figure 5. Calculated equation of state for $LuPO_4$ and $YbPO_4$. V_0 and V_p are the cell volumes at ambient pressure and pressure P respectively.

Table 3. Comparison between the experimental [10] and calculated elastic constants C_{ij} and bulk modulus in GPa units. The experimental data for $LuPO_4$ and $YbPO_4$ are from [10a], and [10b] respectively.

		Zircon		Scheelite
	Elastic constant	Experimental	Calculated	Calculated
$LuPO_4$	C_{11}	320 ± 3	317	373
	C_{33}	382 ± 14	449	195
	C_{44}	84.6 ± 0.8	95	37
	C_{66}	21.7 ± 0.2	24	94
	C_{12}	36 ± 7	56	175
	C_{13}	115 ± 5	158	198
	B		184	195
$YbPO_4$	C_{11}	292 ± 3	314	369
	C_{33}	315 ± 7	445	199
	C_{44}	87 ± 2	94	39
	C_{66}	35 ± 2	23	91
	C_{12}	22 ± 5	54	171
	C_{13}		156	197
	B		181	199

The experimental data of specific heat are not available for $LuPO_4$ and $YbPO_4$. The lattice dynamical model is used for the predictions of specific heat (figure 6). Due to larger volume thermal expansion in the scheelite phase in comparison with the zircon phase (described below), the anharmonic correction (C_P–C_V) is larger for the scheelite phase (figure 6).

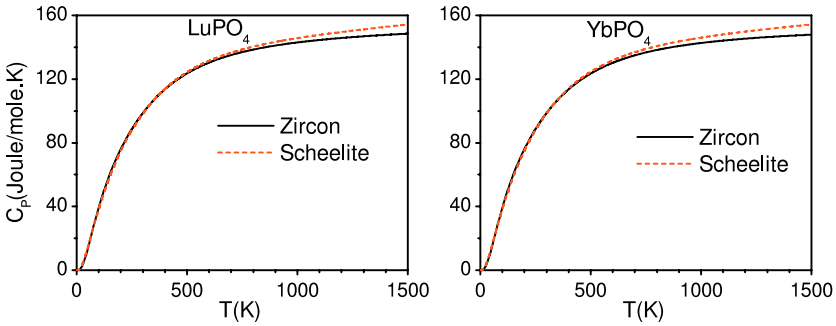

Figure 6. Calculated specific heat in the zircon and scheelite phases of $LuPO_4$ and $YbPO_4$.

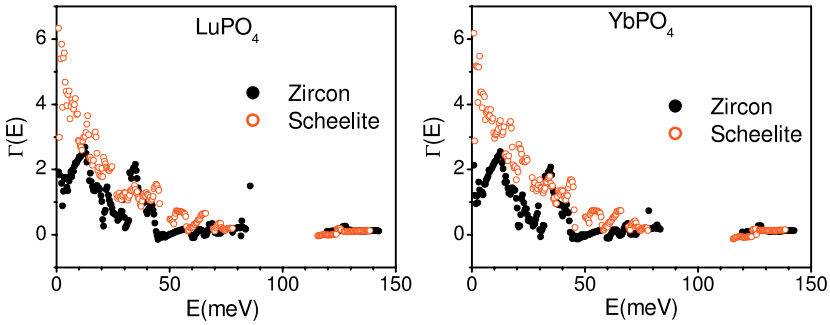

Figure 7. Calculated mode Grüneisen parameter Γ averaged for phonons of energy E in the zircon and scheelite phases of $LuPO_4$ and $YbPO_4$. The value of Γ averaged over the whole Brillouin zone in the zircon (scheelite) phase of $LuPO_4$ and $YbPO_4$ is 0.70 (1.03) and 0.62 (1.11) respectively.

According to the quasiharmonic approximation, thermal expansion [25, 26] is given by

$$\alpha_V = \frac{1}{BV}\sum_i \Gamma_i C_{Vi}(T), \tag{6}$$

where $\Gamma(= -\partial \ln E_i/\partial \ln V)$ and $C_{Vi}(T)$ are the mode Grüneisen parameter and specific heat contributions, respectively, from the phonons in state i $(=\mathbf{q}j)$. We have also included the contribution to thermal expansion arising from variation of the bulk modulus with volume [29, 30]. This procedure is applicable when explicit anharmonicity of phonons (due to thermal amplitudes) is not very significant, and the thermal expansion arises mainly from the implicit anharmonicity, due to the change of phonon frequencies with volume. Figure 7 shows our calculated average Γ values for various phonon energies in zircon and scheelite phases of $LuPO_4$ and $YbPO_4$. Γ values are nearly the same for the isostructural compounds. However, there is a large difference in the calculated Γ values for the zircon and scheelite phases. It can be seen that below 15 meV there are a significant number of modes in the scheelite phase whose Γ values are large in comparison with the zircon phase. The Γ values in the zircon phase lie between -0.2 and 2.8 while in the scheelite phase Γ varies from -0.2 to 6.5. The value of Γ averaged over the whole Brillouin zone in the zircon (scheelite) phase of $LuPO_4$ and $YbPO_4$ is 0.70 (1.03) and 0.62 (1.11) respectively. Figure 8 shows the calculated volume thermal expansion behavior in both the zircon and scheelite phases of $LuPO_4$ and $YbPO_4$. The experimental data of thermal expansion [31], available only for the zircon phase of $LuPO_4$ up to 300 K, show very good agreement with our calculations. Large Γ values in the scheelite phase result in large α_V. Since the model overestimates the bulk modulus of $YbPO_4$ by about

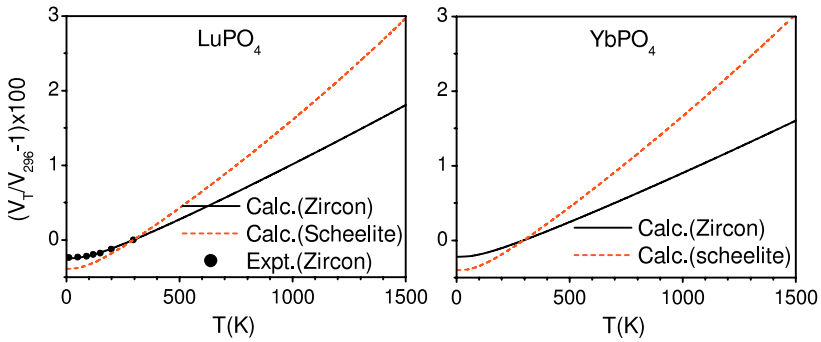

Figure 8. The comparison between the calculated and experimental [31] thermal expansion for $LuPO_4$, $(\frac{V_T}{V_{296}} - 1) \times 100\%$, V_T and V_{296} being the cell volumes at temperatures T and 296 K respectively. The calculated thermal expansion behavior of $YbPO_4$ is also shown.

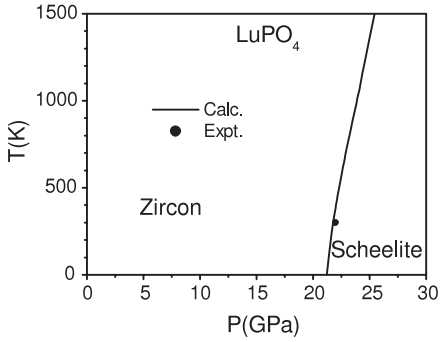

Figure 9. The calculated phase diagram of $LuPO_4$ as obtained from comparison of the calculated free energies in the zircon and scheelite phases of $LuPO_4$. The experimental observation [7] of the phase transition is also shown.

20%, similar discrepancies would occur in the estimates of the equation of states and thermal expansion. However, the prediction of specific heat largely depends on density of states, that is fairly well reproduced by the model.

Several of the zircon structure compounds are known to transform [5–8] to the scheelite phase (figure 1) at high pressure. $LuPO_4$ showed a phase transition [7] at 22 GPa at ambient temperature in Raman scattering experiments carried out at Trombay. The calculated structure of the scheelite phase of $LuPO_4$ is given in table 4. The c/a ratio in scheelite phase is found to be almost twice that of the zircon phase. The Gibbs free energies have been calculated including the vibrational contributions as a function of pressure up to 30 GPa and temperature up to 2000 K in the zircon as well as the high-pressure scheelite phase. A comparison of the free energy diagram suggests that the phase boundary between the low-pressure zircon type and the high-pressure scheelite type occurs at 22 GPa (figure 9), which is in good agreement with the experimental observations [7].

6. Conclusions

We have developed a lattice dynamical model for $LuPO_4$ and validated it by phonon density of states and phonon dispersion relation data available in the literature. The model is then

Table 4. The calculated structure of the scheelite phase of $LuPO_4$ at ambient pressure. For scheelite structure (body-centered tetragonal, $I4_1/a$) the Lu, P and O atoms are located at (0, 0.25, 0.625), (0, 0.25, 0.125) and (u, v, w) respectively and their symmetry equivalent positions. Experimental data are not available for comparison.

	Calculated
a (Å)	4.687
c (Å)	11.061
u	0.266
v	0.871
w	0.559

transferred to $YbPO_4$ by changing only the potential parameter associated with the radius of Yb. The presence of electron–phonon coupling between the rare-earth magnetic moment and the lattice in $YbPO_4$ would influence the low energy phonon density of states. Our lattice dynamics calculations are carried out using an atomistic approach, wherein the effects of interactions between the Yb f electrons and phonons cannot be incorporated. Despite this the calculated phonon density of states for $YbPO_4$ is in fair agreement with our inelastic neutron scattering measurements in the energy range 10–150 meV as carried out using the HRMECS spectrometer at ANL. Further, we employed the lattice dynamical model for calculations of various high pressure and temperature thermodynamic properties of $LuPO_4$ and $YbPO_4$ in the zircon and scheelite phases. Our calculated free energies show a stable zircon structure of $LuPO_4$ below 22 GPa at ambient temperature and a transformation to the scheelite structure at higher pressures, which is in good agreement with the experimental observations.

Acknowledgments

Work performed at Argonne National Laboratory was supported by the US Department of Energy, Office of Science, Office of Basic Energy Sciences, under contract DE-AC02-06CH11357.

References

[1] Boatner L A, Beall G W, Abraham M M, Finch C B, Huray P G and Rappaz M 1980 *The Scientific Basis for Nuclear Waste Management* vol II, ed C J Northrup (New York: Plenum) p 289
[2] Hayhurst T, Shalimoff G, Edelstin N, Boatner L A and Abraham M M 1981 *J. Chem. Phys.* **74** 5449
[3] Milligan W O, Mullica D F, Beall G W and Boatner L A 1983 *Acta Crystallogr.* C **39** 23
[4] Milligan W O, Mullica D F, Beall G W and Boatner L A 1982 *Inorg. Chem. Acta* **60** 39
[5] Duclos S J, Jayaraman A, Cooper G P and Maines R G 1989 *J. Phys. Chem. Solids* **50** 769
[6] Jayaraman A, Kourouklis G A, Espinosa G P and Cooper A S 1987 *J. Phys. Chem. Solids* **50** 759
[7] Rao R, Sakuntala T, Mittal R, Deb S K, Chaplot S L, Karanjikar N P and Roy A P 1998 *Int. Conf. on Raman Scattering (Cape Town, 1998)*
[8] Wang X, Loa I, Syassen K, Hanfland M and Ferrand B 2004 *Phys. Rev.* B **70** 64109
[9] Becker P C, Wiliams G M, Edeldtein N M, Koningstein J A, Boatner L A and Abraham M M 1992 *Phys. Rev.* B **45** 5027
[10a] Armbruster A, Thoma R and Wehrle H 1974 *Phys. Status Solidi* a **24** K71
[10b] Nipko J C, Grimsditch M, Loong C-K, Kern S, Abraham M M and Boatner L A 1996 *Phys. Rev.* B **53** 2286
[11] Loong C-K, Loewenhaupt M, Nipko J C, Braden M and Boatner L A 1999 *Phys. Rev.* B **60** R12549
[12] Begun G M, Beall G W, Boatner L A and Gregor W J 1981 *J. Raman Spectrosc.* **11** 273
[13] Armbruster A 1976 *J. Phys. Chem. Solids* **37** 321
[14] Nipko J C, Loong C-K, Loewenhaupt M, Braden M, Reichardt W and Boatner L A 1997 *Phys. Rev.* B **56** 11584
[15] Mittal R, Chaplot S L, Parthasarathy R, Bull M J and Harris M J 2000 *Phys. Rev.* B **62** 12089

[16] Mittal R, Chaplot S L, Rao Mala N, Choudhury N and Parthasarthy R 1998 *Physica* B **241** 403
[17] Chaplot S L, Pintschovius L, Choudhury N and Mittal R 2006 *Phys. Rev.* B **73** 94308
[18] Chaplot S L, Pintschovius L and Mittal R 2006 *Physica* B **385** 150
[19] Rao K R, Chaplot S L, Padmanabhan V M and Vijayaraghavan P R 1982 *Pramana* **19** 593
Kovalev O V 1964 *Irreducible Representations of Space Groups* (New York: Gordon and Breach)
Bradely C J and Cracknell A P 1972 *The Mathematical Theory of Symmetry in Solids* (Oxford: Oxford University Press)
[20] Price D L and Skold K 1986 *Neutron Scattering* vol A, ed K Skold and D L Price (Orlando, FL: Academic)
Carpenter J M and Price D L 1985 *Phys. Rev. Lett.* **54** 441
Taraskin S N and Elliott S R 1997 *Phys. Rev.* B **55** 117
[21] Chaplot S L, Choudhury N, Ghose S, Rao Mala N, Mittal R and Prabhatasree K N 2002 *Eur. J. Mineral.* **14** 291
[22] Mittal R and Chaplot S L 1999 *Phys. Rev.* B **60** 7234
[23] Mittal R, Chaplot S L and Choudhury N 2001 *Phys. Rev.* B **64** 94302
[24] Mittal R, Chaplot S L and Choudhury N 2006 *Prog. Mater. Sci.* **51** 211
[25] Bruesch P 1982 *Phonons: Theory and Experiments* vol 1 (Berlin: Springer)
[26] Venkatraman G, Feldkamp L and Sahni V C 1975 *Dynamics of Perfect Crystals* (Cambridge, MA: MIT Press)
[27] Chaplot S L 1992 unpublished
[28] Sjolander A 1958 *Ark. Fys.* **14** 315
[29] Jindal V K and Kalus J 1986 *Phys. Status Solidi* b **133** 89
[30] Bhandari R and Jindal V K 1991 *J. Phys.: Condens. Matter* **3** 899
[31] Skanthakumar S, Loong C-K, Soderholm L, Richardson J W Jr, Abraham M M and Boatner L A 1995 *Phys. Rev.* B **51** 5644